SCIENTIFIC REPORTS

OPEN

Phase Stability and Compressibility of 3R-MoN_2 at High Pressure

Xuefeng Zhou[1], Mingqi Yan[1], Mingdong Dong[1], Dejiang Ma[1], Xiaohui Yu[2], Jianzhong Zhang[3], Yusheng Zhao[1] & Shanmin Wang[1]

Received: 24 November 2018
Accepted: 26 June 2019
Published online: 19 July 2019

We report phase stability and compressibility of rhombohedral 3R-MoN_2, a newly discovered layer-structured dinitride, using *in-situ* synchrotron high-pressure x-ray diffraction measurements. The obtained bulk modulus for 3R-MoN_2 is 77 (6) GPa, comparable with that of typical transition-metal disulfides (such as MoS_2). The axial compressibility along *a* axis is more than five times stiffer than that along *c* axis. Such strong elastic anisotropy is mainly attributed to its layered structure with loosely bonded N-Mo-N sandwich interlayers held by weak Van der Waals force. Upon compression up to ~15 GPa, a new hexagonal phase of 2H-MoN_2 occurs, which is irreversible at ambient conditions. The structural transition mechanism between 3R and 2H phases is tentatively proposed to be associated with the rotation and translation of sandwich interlayers, giving rise to different layer stacking sequences in both phases. At high temperature, the decomposition of 3R-MoN_2 leads to the formation of hexagonal δ-MoN and the onset degassing temperature increases as the pressure increases. In addition, the low-temperature electrical resistivity measurement indicates that 3R-MoN_2 behaves as a semiconductor with an estimated band gap of $E_g \approx 0.5$ eV. 3R-MoN_2 also shows weak antiferromagnetic properties, which probably originates from the occurrence of magnetic zigzag edges in the structure.

Transition-metal (TM) nitrides are a class of technologically important compounds and have attracted considerable attention because they exhibit many unique properties and can be used as hard protective coatings (e.g., TiN and CrN)[1], semiconductors (ScN)[2], superconductors (*e.g.*, NbN)[3], and superior catalysts[4,5]. Among TM nitrides, molybdenum nitrides (Mo-N) often exhibit interest properties particularly[4–10]. As a typical example, hexagonal δ-MoN holds the highest hardness in the family of metal nitrides with the second highest superconducting temperature (*i.e.*, $T_c \approx 14$ K)[11]. Thus, the search for new nitrides in the Mo-N system will provide great opportunities for fundamental studies and industrial applications in many fields of science and technology.

However, synthesis of these nitrides is still challenging because the incorporation of nitrogen into the crystalline lattices of transition metals is thermodynamically unfavorable at atmospheric pressure. As a result, most of the reported TM nitrides are poorly crystallized and nitrogen-deficient with molar ratios of N: metal less than unity, which severely limits their use in diverse technological applications. In the binary Mo-N system, three different phases with varying nitrogen concentrations have been reported, referring to ref.[5] for a thorough overview of this system. In spite of the fact that an oxidation state of Mo as high as +6 occurs in other chemical systems (*e.g.*, MoO_3), the synthesis of nitrogen-rich nitride, MoN_2, is still limited by traditional synthetic routes at ambient pressure.

Thanks to recent advancements in high-pressure techniques, a number of novel nitrogen-rich TM nitrides have recently been synthesized from direct metal-gas (N_2) reactions in a pressure range of 18–50 GPa[12]. The new compounds include Th_3P_4-type A_3N_4 (A = Zr and Hf)[13] and noble metal dinitrides (OsN_2, IrN_2, and PtN_2)[14,15]. Successful high-*P* synthesis of nitrides with higher oxidation states demonstrates that pressure can effectively promote the role of *d*-electrons in chemical bonding with nitrogen. Most recently, we have successfully synthesized a series of novel nitrogen-rich tungsten nitrides (*e.g.*, W_2N_3 and W_3N_4) through a newly formulated solid-state ion-exchange reactions between Na_2XO_4 (*X* = Cr, Mo and W) and *h*BN at pressures up to 5 GPa, which is in the pressure range of the current technological capability for massive, industrial-scale production[16,17]. Of particular interest is the discovery of a novel nitrogen-rich nitride, 3R-MoN_2 using this formulated synthesis methodology. Strikingly, the new nitride is explored to adopt a rhombohedral MoS_2-type structure (*i.e.*, a layered structure), which consist typically of one plane of hexagonally packed metal atoms sandwiched by two planes of nitrogen

[1]Department of Physics, Southern University of Science & Technology, Shenzhen, 518055, China. [2]Institute of Physics, Chinese Academy of Sciences, Beijing, 100190, China. [3]Materials Science & Technology Division, Los Alamos National Laboratory, Los Alamos, NM, 87545, USA. Correspondence and requests for materials should be addressed to S.W. (email: wangsm@sustech.edu.cn)

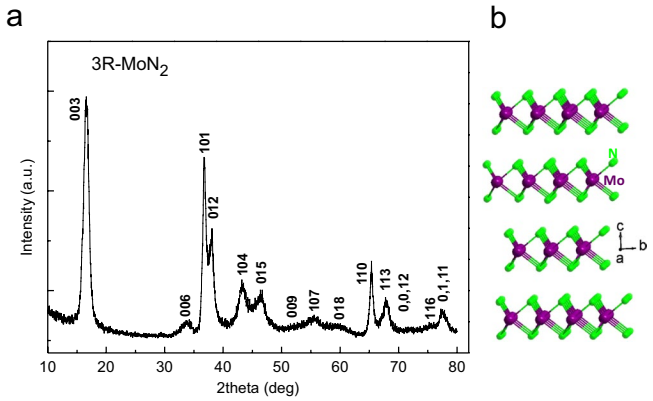

Figure 1. (**a**) X-ray diffraction pattern of rhombohedral 3R-MoN_2 taken at room temperature. (**b**) Crystal structure of 3R-MoN_2 characterized by the stacking of N-Mo-N sandwich layers.

atoms. The sandwich layers are vertically stacked and loosely bonded by weak van der Waals forces as suggested by theoretical simulations[9,18], similar to that in the TM dichalcogenides[19]. Besides, our preliminary experiments indicate that 3R-MoN_2 demonstrates highly catalytic activities for hydrogenation processes, and it may hold great promise as the next-generation catalysts and energy storage materials for a wide range of applications[7,8]. Regarding physical properties of 3R-MoN_2, to date, it has sparsely been explored, but store exciting physics, especially for the material has the form of an atomic-level thin MoN_2 sheet. Remarkably, recent theoretical calculations indicate that the monolayer MoN_2 may have intriguing structural, electronic, and magnetic properties[6,9,18].

For the layer-structured material systems, it often exists a series of different polymorphs such as hexagonal 2H and rhombohedral 3R polytypes as demonstrated in MoS_2[20]. The only structural difference between 2H and 3R phases is their stacking sequences of close-packed sandwich layers. Because of the weak interlayer interaction, both polymorphs can readily be converted between them through the interlayer rotation coupled with translation at certain high pressure and temperature[20]. Apparently, it provides an effective protocol to prepare new polytype 2H-MoN_2 by treating the synthesized 3R-MoN_2 under high pressure conditions. To the best of our knowledge, in addition to its electronic and magnetic properties, the phase stability of the newly synthesized 3R-MoN_2 has not yet been investigated which further limits its industrial applications, calling for more experimental data on this material.

With these aims in this work, we present a comprehensive study on 3R-MoN_2 with focus on the phase stability and compressibility using high-*P* synchrotron XRD measurements, leading to the discovery of a new 2H-MoN_2. The elastic, electronic, and magnetic properties of 3R-MoN_2 have also been explored in detail.

Experimental Section

High-purity Na_2MoO_4 (>99.5%, ~50 μm) and *h*BN (>99.9%, ~50 μm) powders in the molar ratio Na_2MoO_4: BN = 1: 2 were homogeneously mixed for the synthesis of the nitride. High *P-T* synthesis experiments were performed using a DS 6 × 14 MN cubic press and the detailed experimental procedures have previously been described in refs[5,21]. The run products were washed with distilled water to remove the byproduct $NaBO_2$ and unreacted Na_2MoO_4, followed by drying in an oven at 348 K. To obtain phase-pure nitride, a two-step reaction route was adopted, referring to ref.[5] for more experimental descriptions.

High-*P* angle-dispersive synchrotron x-ray diffraction (XRD) experiments using a diamond-anvil cell (DAC) were performed up to 30 GPa at the HPCAT 16BM-D beamline of the Advanced Photon Source (APS). In each of the high-P experiment, the nitride powders with submicron grain size were loaded into the sample hole in a stainless-steel gasket pre-indented to ~30 microns in thickness with neon as the pressure-transmitting medium. A few ruby balls were also loaded into the sample hole to serve as the internal pressure standard. High *P-T* energy-dispersive synchrotron diffraction experiments were performed up to 10 GPa and 1273 K in a large-volume high-*P* apparatus installed at the X17B2 beamline of the National Synchrotron Light Source (NSLS). The experimental details for angle- and energy-dispersive synchrotron measurements have been described previously[16,22]. The crystal structure was determined from analysis of the x-ray data using the GSAS software[23].

Low-*T* magnetic susceptibility and four-probe resistivity measurements were conducted on a bulk sample sintered at 3.5 GPa and 753 K for 8 hours to measure the electric and magnetic properties. The final bulk sample was 4 mm in diameter and 1 mm in thickness. The density of the sintered sample was measured using the Archimedes method, and the obtained value is within more than 90% of the x-ray determined density.

Results and Discussion

Figure 1a shows a typical XRD pattern of the purified product synthesized at 3.5 GPa and 753 K for 20 hours through a step reaction. The refined lattice parameters $a = 2.854$ Å and $c = 15.938$ Å agree well with previously reported values[5]. The crystal structure of the rhombohedral 3R-MoN_2 is shown in Fig. 1b, exhibiting a layered structure similar to that of MoS_2. Figure 2a shows selected high-*P* synchrotron XRD patterns of 3R-MoN_2. During room-temperature compression, a new peak around $2\Theta = 13°$ was observed at ~14.8 GPa, and with further increasing pressure its diffraction intensity increases progressively, indicating the formation of a new MoN_2 phase (also see Fig. S1). The two

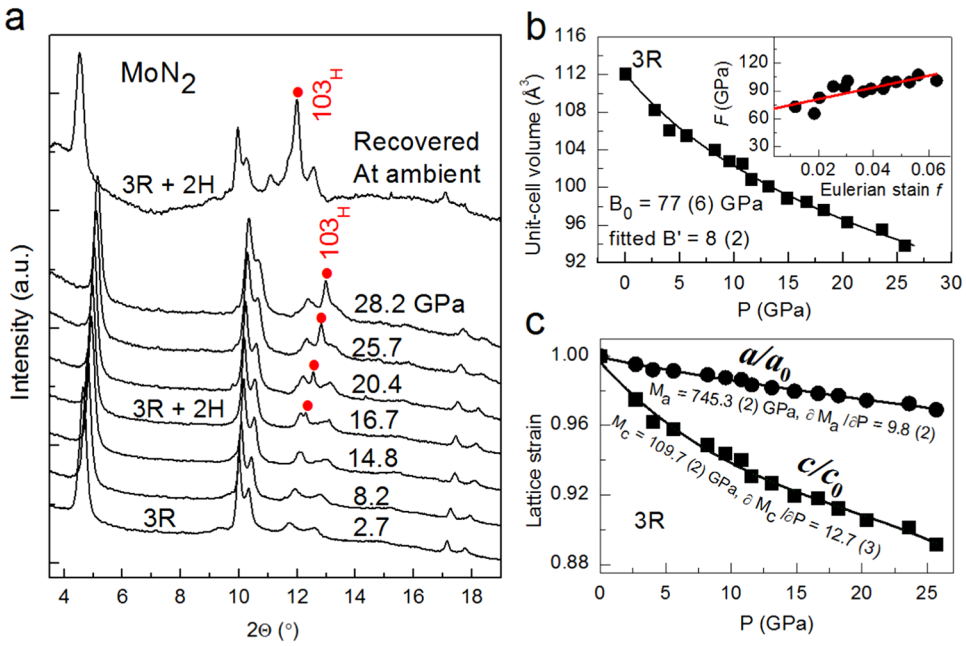

Figure 2. (**a**) Selected high-*P* synchrotron XRD patterns of 3R-MoN_2 upon room-temperature compression in a DAC. The incident x-ray wavelength (λ) is 0.424603 Å. Red dots denote the new Bragg reflection (103) originated from the hexagonal phase. (**b**) Pressure-volume data of 3R-MoN_2 fitted to the 3rd Birch-Murnaghan equation of state. The inset shows the normalized pressure (*F*) as a function of Eulerian strain (*f*). (**c**) Calculated linear elastic moduli along *a*- and *c*-axis for 3R-MoN_2, using the EoSFit program as made by Angel *et al.*[31]. All the error bars in (**b,c**) are too small to be visible.

MoN_2 phases coexist up to the highest experimental pressure of 30 GPa. After the release of the pressure, this phase was recovered at ambient conditions. As will be discussed below, this phase is referred to 2H-MoN_2. Shown in Fig. 2b is the pressure-volume data of 3R-MoN_2 fitted to the 3rd order Birch-Murnaghan equation of state. In the inset, the normalized pressure (*F*) is plotted vs. the Eulerian strain (*f*). The obtained bulk modulus, B_0, is 77 (6) GPa with $B'=8$ (2), indicating that MoN_2 is slightly stiffer than MoS_2 ($B_0 \approx 53$ GPa and $B' \approx 9$)[24]. This difference is likely due to the enhanced cation-anion bonding in the nitride, because compared with sulfur, the nitrogen is more favorable for the formation of strong covalent bonding states with transition metals. In addition, as shown in Fig. 2c, the *c*-axis is substantially more compressible than the *a*-axis, a behavior that is usually expected in the layer-structured materials. Also noted is that the elastic compressibility of the newly formed 2H phase would be similar due to the structural similarity of both phases as will be discussed below.

For the newly emerged phase at high pressure, as mentioned above it is well known that the layer-structured MoS_2 often exists in two different polymorphs: rhombohedral 3R and hexagonal 2H phases; the major difference between them is in the layer stacking sequence[20]. Accordingly, the 2H-MoS_2-type structure with the space group $P6_3/mmc$ was used for analyzing the XRD data of this new MoN_2 phase. As shown in Fig. 3a, the structure refinement shows that the calculated XRD profile is in excellent agreement with the observed data taken at 20.4 GPa with the coexistence of both rhombohedral and hexagonal polytypes. It is noted that the large background of high-P XRD patterns should originate from the sample crystallinity, because the synthesis of high-quality MoN_2 sample is still challenging as descripted in our previous report, referring to ref.[5]. This hexagonal phase is therefore referred to as 2H-MoN_2, and the refined structural parameters are listed in Table 1. The phase transition between 2H- and 3R-MoN_2 is presumably associated with the rotation and translation of N-Mo-N sandwich layers as previously reported in MoS_2[20]. Because of their slight structural difference, it is challenging to distinguish between the 2H and 3R phases using the TEM techniques (Fig. S3). It is found that the pressure-induced phase transition from the rhombohedral 3R-MoN_2 phase to a hexagonal 2H-MoN_2 structure is irreversible, as referred from the experimental and theoretical x-ray diffraction patterns of MoN_2 at ambient conditions in Fig. 3b. Also noted is that the density of high-P 2H phase is anomalously lower than that of 3R-MoN_2 at 20.4 GPa as listed in Table 1. This is not unexpected because the transition from 3R to 2H is often kinetically difficult for achieving a complete conversion; as a result, the final 2H phase would involve a large fraction of the layer stacking disorder and strain in the lattice, which will lead to a significant lattice expansion, hence the reduced the density. For 2H-MoN_2, compared with simulated XRD pattern (see Fig. 3b), a slight peak shift of the 102 and 105 suggests a severe strain or stress that may build up between the interlayer at relatively low pressure. This is because the 2H phase is metastable phase and trends to transform into 3R phase upon decompression, involving a certain degree of the N-Mo-N interlayer rotation and translation. Compared with the 105 reflection, the 102 peak has a large shift relative to the calculated, probably because of the different stress as induced by interlayer stacking disorder involving different number of layers. The similar phenomenon has been observed in refs[5,20]. As depicted in Fig. 3c, the only crystal structural difference between of 3R- and 2H-MoN_2 is the interlayer stacking mode. In fact, for most known layer structured materials, they often adopt a common structure of hexagonal 2H polytype (AB|AB|…) with space

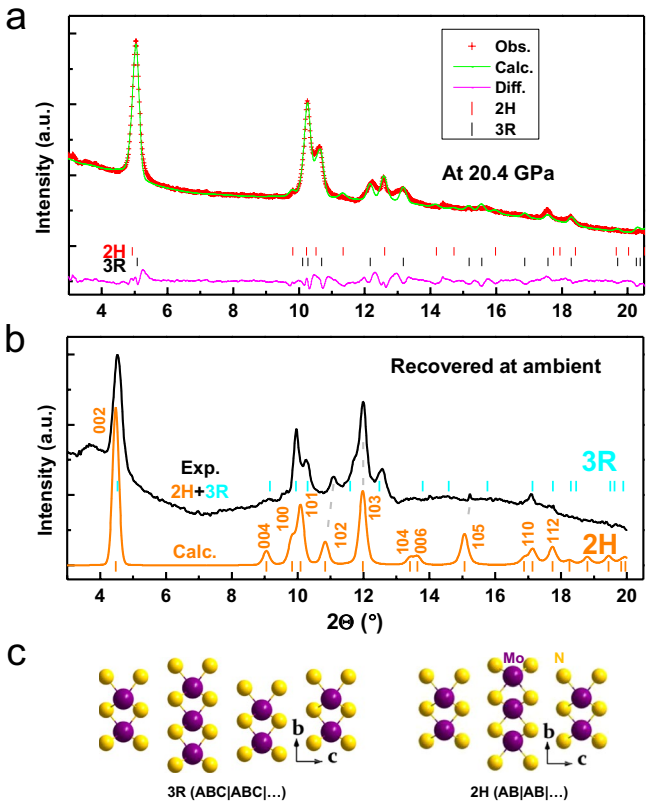

Figure 3. (**a**) Refined XRD pattern for 3R- and 2H-MoN_2 at 20.4 GPa. (**b**) XRD pattern of the recovered sample with coexistence of 3R and 2H phases. In (**a,b**), the incident x-ray wavelength (λ) is 0.424603 Å. (**c**) Comparison of crystal structures between 3R and 2H polymorphs.

	3R-MoN_2		2H-MoN_2
P-T conditions	Ambient	20.4 GPa, 300 K	20.4 GPa, 300 K
Formula	Mo_3N_6		Mo_2N_4
System	rhombohedral		hexagonal
Space group	*R*3m (No. 160)		$P6_3/mmc$ (No. 194)
Cell parameters [Å]	$a=b=2.854$ (1)	$a=b=2.776$ (3)	$a=b=2.757$ (3)
	$c=15.938$ (2)	$c=14.380$ (3)	$c=9.910$ (2)
Cell volume [$Å^3$]	112.42 (4)	95.968 (3)	65.235 (2)
Density [g•cm^{-3}]	5.492 (2)	6.433 (3)	6.310 (2)
Mo Wyckoff site	Mo1: 3*a*, (0, 0, 0.000 (1))		Mo1: 2*c*, (1/3, 2/3, 1/4)[c]
N Wyckoff sites	N1: 3*a*, (0, 0, 0.258 (1)) N2: 3*a*, (0,0,0.402 (2))		N1: 4*f*, (1/3, 2/3, 5/8)[d]
d_{Mo-N} [Å]	1.976, 2.037		
$D_{Interlayer}$ [Å][a]	5.313 (1)		
$D_{Layer\ distance}$ [Å][b]	3.017 (1)		
R_P, wR_P [%] (XRD)[e]	2.1, 3.4	1.7, 2.3	1.7, 2.3
R_P, wR_P [%] (NPD)	3.2, 5.3		
Refs	ref.[4]	This study	This study

Table 1. Summary of structural parameters for MoN_2 phases determined by analyses of x-ray and neutron diffraction data. [a,b]$D_{Interlayer}$ is the distances between the two nearest neighboring Mo planes, and $D_{Layer\ distance}$ corresponds to the distance between the N planes. [c,d]Proposed atomic positions for 2H-MoN_2, which cannot be refined accurately using the current high-*P* XRD data. [e]R_P and wR_P represent the profile residual and the weighted profile R-factor of refined XRD patterns.

group of $P6_3/mmc$ (No. 194), including TM dichalcogenides TMX_2 (TM = Nb, Mo, Ta, and W; *X* = S and Se). In contrast, the 3R rhombohedral polytype (ABC|ABC|…) is a high-temperature phase with a space group of *R*3*m* (No. 160)[25,26]. Therefore, 3R-MoN_2 may be a high-T phase with a space group of R3m (No. 160), compared with 2H-MoN_2 with a space group of P63/mmc (No. 194)[18,25].

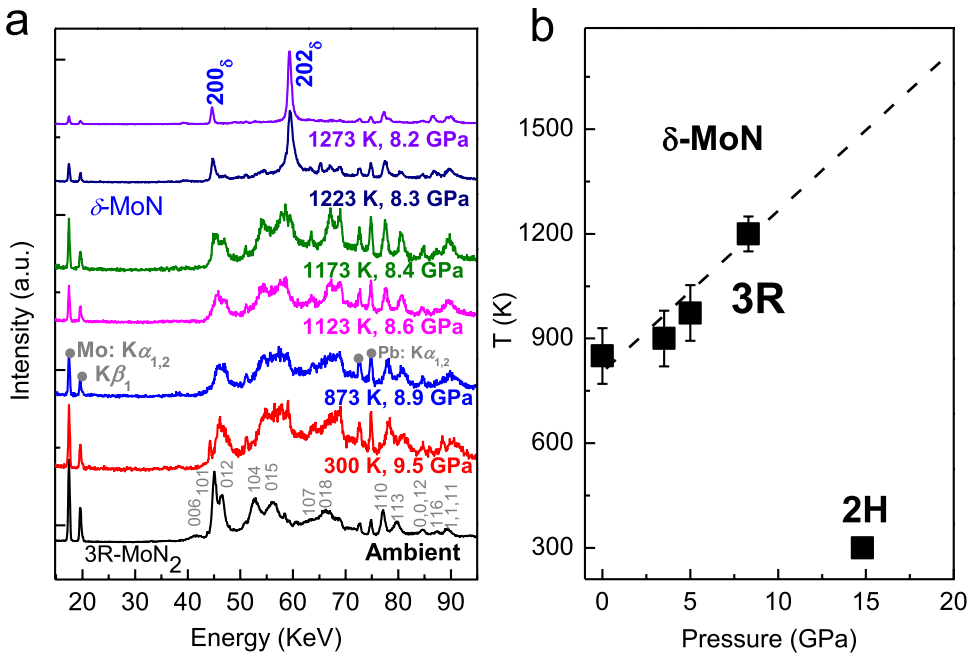

Figure 4. (**a**) *In situ* high P-T energy-dispersive synchrotron XRD measurements. Fluorescence peaks of Mo: $K_{\alpha,\beta}$ and Pb: K_{α} are denoted by grey solid dots, which originate from MoN_2 and lead shielding of the detector, respectively. (**b**) Thermal stability of 3R as a function of pressure. δ-MoN forms through the degassing of 3R-MoN2 at high temperature.

To study the phase stability at high temperature, we performed *in-situ* energy-dispersive high *P-T* synchrotron XRD measurement using a large volume pressure. As shown in Fig. 4a, the XRD patterns were collected on heating at a constant load of 80 ton. Because of the thermal effect of the sample cell, the corresponding pressure decreases from 9.5 GPa at 300 K to 8.2 GPa at 1273 K. The strongest Bragg reflection (003) of 3R-MoN_2 is located at the low-energy region, and it is thus undetectable by the energy-dispersive XRD measurement. Clearly, *δ*-MoN is formed at ~1200 (20) K and 8.3 GPa through nitrogen degassing of 3R-MoN_2. The decomposition process is expressed by,

$$MoN_2 = MoN + 1/2\ N_2 \quad (1)$$

The phase stability of 3R-MoN_2, however, is substantially enhanced with increasing pressure, leading to highly increased N_2 decomposing temperature (see Fig. 4b). At 8.3 GPa, for example, the reaction (1) happens at a higher temperature of ~1200 K based on *in-situ* high *P-T* synchrotron XRD measurement. The phase diagram of MoN_2 is eventually determined and summarized in Fig. 4b. Apparently, at high temperature, the *δ*-MoN can be formed through nitrogen degassing of 3R-MoN_2, on the basis of our previous study of this material in ref.[5]. However, it is experimentally difficult to determine the phase boundary between 2H and 3R at high temperatures above 15 GPa. Nevertheless, the 3R phase seems thermodynamically more stable than 2H phase at high temperature as shown in Fig. 4b. Further experimental work is warranted to determine the detailed phase boundary between 3R and 2H using the state-of-the-art high-P techniques.

Figure 5 shows the magnetic and electrical resistivity measurements. At first glance, the low-*T* magnetic susceptibility (χ) data plotted in Fig. 5a suggests a weak paramagnetic-like behavior, as also reported in Li*X*N_2 (*X* = Mo and W)[27,28]. However, after further analyses, the data can be fitted to the Curie-Weiss law in two temperature ranges, 130–300 K and 2–30 K. The obtained Weiss constants are $T_{\Theta} = -283$ (10) K and −6 (2) K, respectively, indicating that there exist two weakly antiferromagnetic (AFM-I and -II) phases for 3R-MoN_2. The corresponding magnetic moments of Mo atom are $\mu_{eff} = 0.12$ (1) and 0.05 (1) μ_B/f.u. Such weak antiferromagnetism in 3R-MoN_2 presumably originates from the magnetic zigzag edges at the grain boundaries as reported for MoS_2[29]. The detailed magnetic measurements are listed in Table 2. Moreover, it is worthwhile to mention that the atomically-thin MoN_2 layers possess intrinsic high-T ferromagnetic properties on the basis of recent *ab-initial* calculations[18], which may be closely associated with the observed magnetism in this work.

As shown in Fig. 5b, the electrical resistivity of 3R-MoN_2 increases dramatically as temperature decreases, which is characteristic of a semiconductor. Based on the typical law for a semiconductor, $\rho(T) = \rho_0 e^{(E_g/2k_BT)}$, a linear fit of the ln$\rho$ - 1/*T* data yields a narrow band gap of $E_g = 0.50$ (1) eV, which is comparable to the value of 0.47 eV for PbS[30]. However, it is substantially smaller than that of MoS_2, an indirect semiconductor with $E_g \approx 1.2$ eV[29]. In contrast, $LiMoN_2$ and $LiWN_2$ both behave as an intrinsic metal; the two ternary nitrides also adopt the 3R symmetry of its parent MoN_2 with intercalated Li layers[27,28]. The measured semiconductor-like behavior in 3R-MoN_2 may be partially associated with the degrees of crystallinity and defects, such as layer stacking faults. Hence, further resistivity measurements on well-crystallized samples are warranted to clarify this issue.

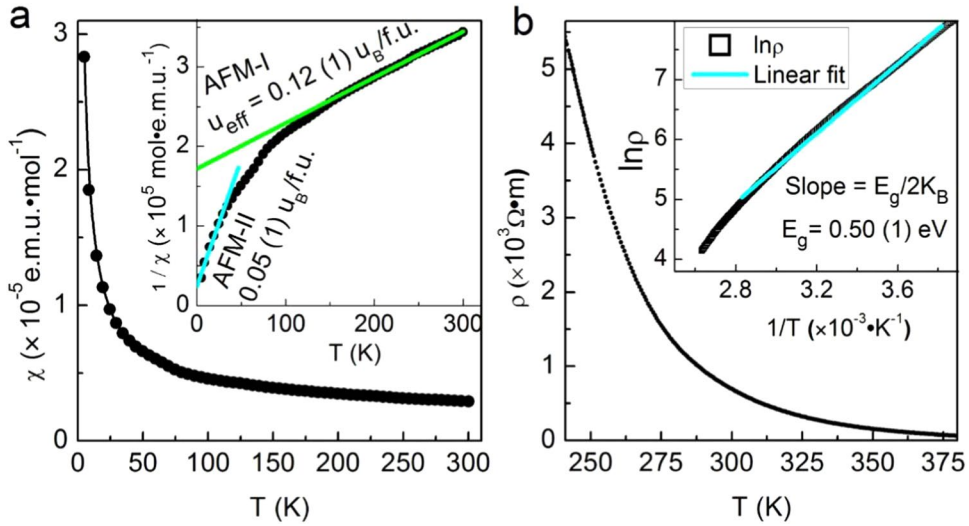

Figure 5. (**a**) Magnetic susceptibility as a function of temperature. The measurements were performed in an external magnetic field of $H = 1000$ Oe. The inset shows the inverse susceptibility, $1/\chi$, against T. It seems both AFM phases coexist in the 30–130 K temperature range. (**b**) Four-point probe resistivity as a function of temperature. The measurements were conducted on a well-sintered bulk sample. The inset shows a linear fit of lnρ vs. 1/T based on the expression $\rho(T) = \rho_0 e^{(E_g/2k_BT)}$, which yields a band gap of $E_g = 0.50$ (1) eV.

	AFM-I	AFM-II
Temperatures [K]	130–300	2–30
Curies constant, C [10^{-3}emu·mol^{-1}·K]	1.69 (1)	0.29 (1)
Weiss constant, T_Θ [K]	−283 (10)	−6 (2)
Magnetic moment, μ_{eff} [μ_B/f.u.]	0.12 (1)	0.05 (1)

Table 2. Magnetic parameters of 3R-MoN_2 derived from the magnetic susceptibility measurements. The magnetic susceptibility data were fitted to the Curie-Weiss law $\chi = C/(T - T_\Theta)$ in two different temperature ranges of 130–300 K and 2–30 K.

Conclusions

In summary, the structural stability and compressibility of a newly discovered layer-structured rhombohedral 3R-MoN_2 have been studied using high-P compression measurements. A recoverable 2H–MoN_2, isotypic with hexagonal MoS_2, is also discovered via high–pressure processing of 3R–MoN_2, probably involving the interlayer rotation and translation as reported in MoS_2. Because of their structural similarity, the obtained bulk modulus and axial compressibility for 3R–MoN_2 are comparable to those of MoS_2. The obtained the bulk modulus for 3R-MoN_2 is $B = 77(6)$ GPa and the axial compressibility along c axis is much softer than that along a axis, confirming that the sandwich interlayers are loosely bonded by Van der Waals force. At a high temperature exceeding ~873 K, 3R-MoN_2 transforms into hexagonal δ-MoN through the degassing of N_2 and this disassociation temperature increases as pressure increases. Besides, 3R-MoN_2 is weakly antiferromagnetic, may resulting from the occurrence of magnetic zigzag edges in the structure. Moreover, the nitride behaves as a semiconductor with $E_g = 0.50(1)$ eV.

References

1. Navinšek, B., Panjan, P. & Cvelbar, A. Characterization of low temperature CrN and TiN (PVD) hard coatings. *Surf. Coat. Technol.* **74–75**(0), 155–161 (1995).
2. Gall, D., Petrov, I., Madsen, L. D., Sundgren, J. E. & Greene, J. E. Microstructure and electronic properties of the refractory semiconductor ScN grown on Mg0(001) by ultra-high-vacuum reactive magnetron sputter deposition. *J. Vac. Sci. Technol. A.* **16**(4), 2411–2417 (1998).
3. Bailey, E. & McMillan, P. F. High pressure synthesis of superconducting nitrides in the MoN-NbN system. *J. Mater. Chem.* **20**(20), 4176–4182 (2010).
4. Wang, S. *et al*. Synthesis of Onion-Like δ-MoN Catalyst for Selective Hydrogenation. *J. Phys. Chem. C.* **121**(35), 19451–19460 (2017).
5. Wang, S. *et al*. A new molybdenum nitride catalyst with rhombohedral MoS_2 structure for hydrogenation applications. *J. Am. Chem. Soc.* **137**(14), 4815–4822 (2015).
6. Zhang, C., Liu, J., Shen, H., Li, X.-Z. & Sun, Q. Identifying the Ground State Geometry of a MoN2 Sheet through a Global Structure Search and Its Tunable p-Electron Half-Metallicity. *Chem. Mater.* **29**(20), 8588–8593 (2017).
7. Li, Q., He, L., Sun, C. & Zhang, X. Computational Study of MoN2 Monolayer as Electrochemical Catalysts for Nitrogen Reduction. *J. Phys. Chem. C.* **121**(49), 27563–27568 (2017).
8. Zhang, X. *et al*. Theoretical prediction of MoN2 monolayer as a high capacity electrode material for metal ion batteries. *Journal of Materials Chemistry A*. **4**(39), 15224–15231 (2016).

9. Wang, Y., Wang, S.-S., Lu, Y., Jiang, J. & Yang, S. A. Strain-Induced Isostructural and Magnetic Phase Transitions in Monolayer MoN_2. *Nano Lett.* **16**(7), 4576–4582 (2016).
10. Cao, B., Neuefeind, J. C., Adzic, R. R. & Khalifah, P. G. Molybdenum Nitrides as Oxygen Reduction Reaction Catalysts: Structural and Electrochemical Studies. *Inorg. Chem.* **54**(5), 2128–2136 (2015).
11. Wang, S. *et al*. The Hardest Superconducting Metal Nitride. *Scientific reports.* **5**(13733), 1–4 (2015).
12. Salamat, A., Hector, A. L., Kroll, P. & McMillan, P. F. Nitrogen-rich transition metal nitrides. *Coord. Chem. Rev.* **257**(13–14), 2063–2072 (2013).
13. Zerr, A., Miehe, G. & Riedel, R. Synthesis of cubic zirconium and hafnium nitride having Th_3P_4 structure. *Nature Mater.* **2**(3), 185–189 (2003).
14. Young, A. F. *et al*. Synthesis of novel transition metal nitrides IrN_2 and OsN_2. *Phys. Rev. Lett.* **96**(15501), 1–4 (2006).
15. Crowhurst, J. C. *et al*. Synthesis and characterization of the nitrides of platinum and iridium. *Science.* **311**(5765), 1275–1278 (2006).
16. Wang, S. *et al*. Experimental invalidation of phase-transition-induced elastic softening in CrN. *Phys. Rev. B.* **86**(6), 064111 (2012).
17. Chen, M., Wang, S., Zhang, J., He, D. & Zhao, Y. Synthesis of stoichiometric and bulk CrN through a solid-state ion-exchange reaction. *Chem. Eur. J.* **18**(48), 15459–15463 (2012).
18. Wu, F. *et al*. Atomically Thin Transition-Metal Dinitrides: High-Temperature Ferromagnetism and Half-Metallicity. *Nano Lett.* **15**(12), 8277–8281 (2015).
19. Benavente, E., Santa Ana, M. A., Mendizábal, F. & González, G. Intercalation chemistry of molybdenum disulfide. *Coord. Chem. Rev.* **224**(1–2), 87–109 (2002).
20. Wang, S. *et al*. Sulfur-catalyzed phase transition in MoS_2 under high pressure and temperature. *J. Phys. Chem. Solids.* **75**(1), 100–104 (2014).
21. Wang, S., He, D., Wang, W. & Lei, L. Pressure calibration for the cubic press by differential thermal analysis and the high-pressure fusion curve of aluminum. *High Pressure Res.* **29**(4), 806–814 (2009).
22. Wang, S. *et al*. Synthesis, Crystal Structure, and Elastic Properties of Novel Tungsten Nitrides. *Chem. Mater.* **24**(15), 3023–3028 (2012).
23. Toby, B. H. EXPGUI, a graphical user interface for GSAS. *J. Appl. Cryst.* **34**, 210–213 (2001).
24. Aksoy, R. *et al*. X-ray diffraction study of molybdenum disulfide to 38.8 GPa. *J. Phys. Chem. Solids.* **67**(9–10), 1914–1917 (2006).
25. Merrill, L. Behavior of the AB[sub 2]-Type Compounds at High Pressures and High Temperatures. *J. Phys. Chem.* **11**(4), 1005–1064 (1982).
26. Silverma, M. S. Ultrahigh pressure-high temperature synthesis of rhombohedral dichalcogenides of molybdenum and tungsten. *Inorg. Chem.* **6**(5), 1063 (1967).
27. Elder, S. H. *et al*. Lithium molybdenum nitride ($LiMoN_2$): the first metallic layered nitride. *Chem. Mater.* **4**(4), 928–937 (1992).
28. Herle, P. S., Hegde, M. S., Vasanthacharya, N. Y., Gopalakrishnan, J. & Subbanna, G. N. Synthesis, structure, and properties of $LiWN_2$. *J. Solid State Chem.* **112**(1), 208–210 (1994).
29. Tongay, S., Varnoosfaderani, S. S., Appleton, B. R., Wu, J. & Hebard, A. F. Magnetic properties of MoS_2: Existence of ferromagnetism. *Appl. Phys. Lett.* **101**(123105), 1–4 (2012).
30. Wang, S. *et al*. Phase-transition induced elastic softening and band gap transition in semiconducting PbS at high pressure. *Inorg. Chem.* **52**(15), 8638–8643 (2013).
31. Angel, R. J. Equations of State. *Reviews in Mineralogy and Geochemistry.* **41**(1), 35–59 (2000).

Acknowledgements

This work is supported by the Guangdong Innovative & Entrepreneurial Research Team Program (No. 2016ZT06C279), the Shenzhen Peacock Plan (No. KQTD2016053019134356), the Shenzhen Development and Reform Commission Foundation for Novel Nano-Material Sciences and the Research Platform for Crystal Growth & Thin-Film Preparation at SUSTech. Portions of this work were performed at HPCAT, Advanced Photon Source (APS), Argonne National Laboratory. HPCAT operations are supported by DOE-NNSA under Award No. DE-NA0001974 and DOE-BES under Award No. DE-FG02-99ER45775, with partial instrumentation funding by NSF. APS is supported by DOE-BES, under Contract No. DE-AC02-06CH11357. Use of the National Synchrotron Light Source (at X17B2 beamline), Brookhaven National Laboratory, was supported by DOE-BES, under Contract No. DE-AC02-98CH10886.

Author Contributions

S.W. and Y.Z. designed research; X.Z. and D.M. performed high-pressure synthesis; X.Y. did low-temperature magnetic and electrical resistivity measurements; J.Z. and X.Z performed high P-T synchrotron XRD measurement. X.Z. prepared Figures 1–5 and wrote the main manuscript text. All authors reviewed the manuscript.

Additional Information

Supplementary information accompanies this paper at https://doi.org/10.1038/s41598-019-46822-4.

Competing Interests: The authors declare no competing interests.

Publisher's note: Springer Nature remains neutral with regard to jurisdictional claims in published maps and institutional affiliations.